

Lagrangian analysis of intermittent sound sources in the flow-field of a bluff-body stabilized combustor

Cite as: Phys. Fluids **31**, 025115 (2019); <https://doi.org/10.1063/1.5064862>

Submitted: 09 October 2018 . Accepted: 26 January 2019 . Published Online: 21 February 2019

C. P. Premchand , Nitin B. George , Manikandan Raghunathan , Vishnu R. Unni , Raman I. Sujith , and Vineeth Nair 



View Online



Export Citation



CrossMark

ARTICLES YOU MAY BE INTERESTED IN

[Coupled interaction between unsteady flame dynamics and acoustic field in a turbulent combustor](#)

Chaos: An Interdisciplinary Journal of Nonlinear Science **28**, 113111 (2018); <https://doi.org/10.1063/1.5052210>

[Flame blowout: Transition to an absorbing phase](#)

Chaos: An Interdisciplinary Journal of Nonlinear Science **28**, 113121 (2018); <https://doi.org/10.1063/1.5045808>

[On the emergence of critical regions at the onset of thermoacoustic instability in a turbulent combustor](#)

Chaos: An Interdisciplinary Journal of Nonlinear Science **28**, 063125 (2018); <https://doi.org/10.1063/1.5028159>



Lagrangian analysis of intermittent sound sources in the flow-field of a bluff-body stabilized combustor

Cite as: Phys. Fluids 31, 025115 (2019); doi: 10.1063/1.5064862

Submitted: 9 October 2018 • Accepted: 26 January 2019 •

Published Online: 21 February 2019



C. P. Premchand,^{1,a)} Nitin B. George,² Manikandan Raghunathan,² Vishnu R. Unni,² Raman I. Sujith,² and Vineeth Nair¹

AFFILIATIONS

¹Department of Aerospace Engineering, Indian Institute of Technology—Bombay, 400076 Mumbai, India

²Department of Aerospace Engineering, Indian Institute of Technology—Madras, 600036 Chennai, India

^{a)} Author to whom correspondence should be addressed: premchand.iitb@gmail.com and prem.aero@iitb.ac.in

ABSTRACT

Experiments were performed in a partially premixed bluff-body stabilized combustor in the regimes of combustion noise, intermittency, and thermoacoustic instability. Simultaneous measurements of unsteady pressure fluctuations and flow-field using time-resolved two-component particle image velocimetry reveal dominant dynamics at 141.9 Hz which is responsible for thermoacoustic instability. In the intermittent regime that presages thermoacoustic instability, there are two distinct frequencies: a low-frequency component at 30.7 Hz dominant in the velocity spectra (hydrodynamic mode) and a higher frequency component at 176.4 Hz dominant in the pressure spectra (acoustic mode). Examining the phase relationship between the two modes in the intermittent regime using a variant of the Dynamic Mode Decomposition (DMD) confirms that the appearance of bursts of periodic pressure oscillations coincide with the time instants when the hydrodynamic and the acoustic modes are phase synchronized. To identify the flow structure dynamics observed only during sound production, we compute ridges in the fields of backward-time finite time Lyapunov exponents. The roll up of shear layers from the dump plane and the leading edge of the bluff body and subsequent impingement on combustor walls are identified as the dominant features of the flow during thermoacoustic instability as well as during the bursting stage of intermittency. We show convincingly that these identified dynamics correspond to the acoustic mode using DMD filtered flow fields comprising only of the acoustic mode.

Published under license by AIP Publishing. <https://doi.org/10.1063/1.5064862>

I. INTRODUCTION

Thermoacoustic instabilities remain an unsolved problem in the past few decades, remaining one of the greatest hurdles in the development of lean premixed combustors.¹ Unsteady combustion results in fluctuations of heat release rate which produce acoustic pressure fluctuations in the combustor. These pressure fluctuations reflect off the boundaries of the combustor and in turn act as sources of additional heat release rate fluctuations.² When the operating conditions are such that the heat release rate fluctuations are in phase with the acoustic pressure pulsations, a positive feedback loop is

established wherein the pressure fluctuations in the combustor are amplified—a phenomenon termed thermoacoustic instability or combustion instability.³

Thermoacoustic instability is undesirable in combustors as it often leads to engine failure. Even when the amplitude of acoustic oscillations is low, such instabilities affect the structural integrity of the engine through fatigue. Thermoacoustic instability also leads to increased heat transfer to the walls of the combustion chamber.² Gas turbine manufacturers thus suffer huge financial losses in repair and replacement of the components due to wear and tear resulting from such instabilities. In addition to these costs, manufacturers of

land-based gas turbine power plants also have to pay for the losses incurred due to power outages arising from thermoacoustic instabilities.⁴ Therefore, researchers are actively seeking methods to forewarn and mitigate their occurrence in fielded combustion systems well before onset.

The operational regime of a turbulent bluff-body stabilized combustor from stable to unstable operation can be split into three regimes based on the dynamics: combustion noise, intermittency, and combustion instability.⁵ For a stable bluff-body stabilized combustor operating at equivalence ratios close to unity, the dynamics comprises mostly of low-amplitude aperiodic fluctuations.⁶ Tony *et al.*⁷ and Nair *et al.*⁸ analyzed the pressure signals acquired during stable operation in a turbulent combustor and found that combustion noise is a high dimensional chaotic regime. Such chaotic regimes were also previously reported prior to periodic oscillations in a lean-premixed gas-turbine combustor.⁹ As the equivalence ratio is decreased from unity, intermittent, periodic burst oscillations start appearing in pressure traces almost randomly in-between regimes of aperiodic, low-amplitude oscillations. When equivalence ratio is decreased even further, dynamics transform completely to a regime of periodic oscillations due to the onset of thermoacoustic instability.¹⁰

Since intermittent burst oscillations often presage thermoacoustic instability in combustors operating in turbulent regimes, several precursors to instability were prescribed by quantifying the intermittent regime. There is a gradual loss of chaos as the dynamics transition from low-amplitude combustion noise regime to high-amplitude combustion instability. This loss can be quantified using 0-1 test which serves as a precursor to thermoacoustic instability.^{7,8} Recurrence properties of the intermittent bursts can be quantified by tracking the distribution of aperiodic segments in the pressure signal which also provides early warning to combustion instability.⁶ Further, the transition to combustion instability also leads to a collapse in the number of relevant time scales in the dynamics. Such a collapse of multifractal spectrum can be quantified using a parameter known as the generalized Hurst exponent which also acts as a precursor measure for the onset of thermoacoustic instability.^{6,11} The results from these studies are summarized in Juniper and Sujith.¹²

Although precursors indicate the proximity of the dynamics to combustion instability, they do not provide any scope for passive or active control as the sound sources, which are ultimately present in the flow-field, are largely unknown. It is observed that in turbulent combustors, large coherent structures¹³ are present in the flow-field that often create periodic pulsations in heat release rate, thereby acting as potential sound sources.¹⁴⁻¹⁹ In other words, control of thermoacoustic instability in such situations is intimately linked to the identification of sound producing coherent structures. Once such structures are identified, we can implement a control framework to suppress the large amplitude pressure pulsations or design a combustor to avoid thermoacoustic instability by targeting and disrupting the sound producing coherent structures. In the present manuscript, we propose Lagrangian

Coherent Structures (LCS) as an indicator of the organized structures present in the flow-field.

Lagrangian coherent structures (LCS) are locally the most repelling and attracting material surfaces in a flow-field and provide a new way of understanding mixing and transport phenomenon in complex fluid flows.²⁰ Introduced by Haller,²¹ LCS has been applied to many fields such as oceanography,²² biological feeding,²³ aerodynamics,²⁴ aeroacoustics,²⁵ and granular flow applications.²⁶ A simple, heuristic way to obtain LCS from a given flow-field is through the computation of fields of finite time Lyapunov exponents (FTLEs). FTLE is a measure of the rate of separation of two adjacent fluid particles after a specified finite time as a function of their initial positions and initial time in the flow field. Ridges or contours of maximum values in the FTLE fields as the particles advect in time are therefore indicators of Lagrangian coherent structures in the flow-field.²⁷

LCS extracted using the FTLE framework has recently been applied to the flow field obtained experimentally from a backward facing step combustor.²⁸ Saddle-type flows were identified that separates the dynamics between the shorter and longer combustor lengths. They show that the FTLE ridges reveal relatively small-scale structures in addition to the large-scale coherent structures. In typical stable combustor flow-fields, especially in the intermittent regimes, several dominant frequencies are present, one of which eventually locks-in with the acoustic field of the combustion chamber during thermoacoustic instability, as the flow conditions are varied. A direct computation of the FTLE fields, however, provides only an overall picture of the structures at all the frequencies in the combustor whose individual contribution to the dynamics is time-dependent and hence an unknown. In other words, the FTLE framework, in isolation, cannot extract the LCS at a particular frequency from the total velocity field unless the dynamics are completely dominated by a single time scale. This highly limits the practical utility of FTLE, especially in identifying coherent structures responsible for sound production at an early stage.

In order to compensate this shortcoming, we propose the well-known flow-decomposition technique of Dynamic Mode Decomposition (DMD) to decompose the dynamics of structures at a particular frequency.²⁹ DMD is an algorithm that reduces the dimensionality of a system whilst preserving as much information in the original data set as possible; i.e., it reduces and extracts the features present in the overall flow-field into a set of basis functions or DMD modes. Once the flow decomposition is performed using DMD into various modes—each of which corresponds to one of the dominant frequencies—FTLE fields can be used to identify coherent structures at a particular frequency of interest in a regime where that frequency is dominant.

The primary objective of this manuscript is, therefore, to provide a framework to identify the mechanism or the feedback loop responsible for thermoacoustic instability by inspecting the flow-fields in the intermittent regime that presages the regime of thermoacoustic instability. In Sec. II,

we outline the experimental setup and data acquisition techniques employed in our study. The methodology used to extract the coherent structures and DMD time coefficients from the flow field is explained in Sec. III. Results and analysis are presented in Sec. IV, and conclusions are summarized in Sec. V.

II. EXPERIMENTAL SETUP

We use a turbulent dump combustor, with the flame stabilized on a bluff body (refer to Fig. 1). The bluff-body is a circular disk of 10 mm thickness and has a diameter of 47 mm located 45 mm from the dump plane. A hollow central shaft of 16 mm diameter mounts the bluff body. The central shaft is also used to deliver the fuel through four radial injection holes of 1.7 mm located 110 mm upstream of the dump plane. Air enters the plenum chamber and mixes with the fuel in the burner before entering the combustion chamber. Liquid petroleum gas (LPG), with a composition of 60% propane and 40% butane by volume, is used as fuel. An 11 kV ignition transformer connected to a spark plug mounted on the dump plane ignites the combustible mixture. The cross-section of the combustion chamber is $90 \times 90 \text{ mm}^2$ and with a length of 1100 mm. Acoustic radiation losses are minimized by using a decoupler which is a large chamber of size $1000 \text{ mm} \times 500 \text{ mm} \times 500 \text{ mm}$ at the end of the combustion chamber. The decoupler also approximately achieves the acoustic boundary condition of an open duct ($p' = 0$).

Mass flow controllers (Alicat Scientific, MCR Series) which have an uncertainty of $\pm 0.8\%$ of the reading $+0.20\%$ of full scale are used for controlling the air and fuel flow rates. This results in an uncertainty of ± 0.02 in the equivalence ratio. A piezoelectric transducer (PCB103B02 uncertainty $\pm 0.15 \text{ Pa}$) mounted on the combustor wall at a distance of 40 mm from

the dump plane measures the unsteady pressure fluctuations. The signals from the piezoelectric transducer are acquired at a sampling rate of 10 kHz, for 3 s using an A-D card (NI-6143, 16 bit). The transducer is not flush mounted, which creates an acoustic phase delay of 5° . However, this phase delay is not large enough to affect the analysis and results presented in this study.

A single cavity-double pulsed Nd:YLF laser (Photonics) of operating wavelength 527 nm is used for the velocity-field measurements. We operate the laser at a repetition rate of 2 kHz. The laser beam is steered towards the combustion chamber using right angle prisms and convex lenses. Subsequently, it is expanded into a laser sheet, which is of 2 mm thickness, using 600 mm spherical and -16 mm cylindrical lenses. Next, it is transmitted through a horizontal slit of 5 mm width, made of quartz, into the combustion chamber to illuminate the seeding particles in the center-span of the bluff body. The Mie-scattered light is captured using a high-speed CMOS camera (Photron FASTCAM SA4). The camera is outfitted with a ZEISS 100 mm lens with an aperture at $f/5.6$. A short band-pass optical filter, centered at 527 nm and mounted in front of the lens, captures the scattered light. The camera is operated at a framing rate of 2 kHz and a resolution of 510×1024 pixels capturing a test section area of $32 \text{ mm} \times 64 \text{ mm}$. The scattered light from the seeding particles is distributed over 1.5–2.5 pixels. This results in a measurement uncertainty of less than 0.03 pixels for this range of particle image diameters.³¹ The time delay between the two laser pulses is set between 15 and $25 \mu\text{s}$ for various flow rates to obtain a maximum pixel displacement between 4 and 7 pixels. The average particle image density is approximately 4 particles per interrogation window in the recirculation (low velocity) regions and 9 particles per interrogation window for the bulk flow (high velocity) regions. TiO_2 particles (Kronos make-product

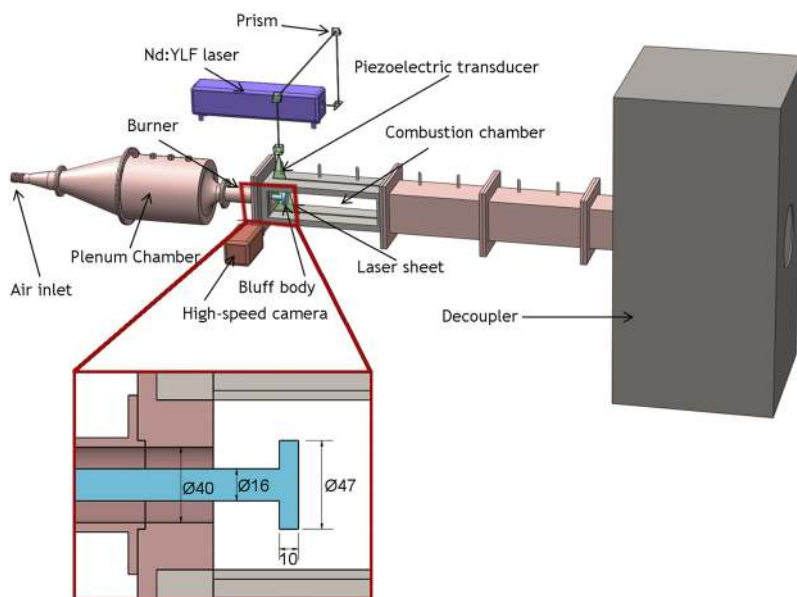


FIG. 1. Schematic of the turbulent bluff-body stabilized combustor used in the study. Design of this combustor was adapted from Komarek and Polifke.³⁰ A piezoelectric pressure transducer placed 40 mm from the dump plane is used to measure the unsteady pressure fluctuations in the combustor. Two-component particle image velocimetry (2C-PIV) experiments are performed using an Nd:YLF laser and a high-speed camera. Geometry of the bluff-body and the burner upstream are shown in the inset.

–1071) of approximate size $1\ \mu\text{m}$ are used as seeding particles (80% of the particles are between the size of $0.2\ \mu\text{m}$ and $2\ \mu\text{m}$). The median of the size of the particles is $0.61\ \mu\text{m}$. The test section window gets clouded quickly due to the small size of the particles. This limits the seeding density and the data recorded for each run of the experiments. The Stokes number for the TiO_2 particles used in our study is approximately 0.0007. In our experiments, the particle phase is not in a dilute form but rather as a suspension. Hence, there could be two-way coupling effects³² where the particles could affect the flow dynamics, where the volume fraction between the dispersed phase and carrier phase is between 10^{-6} and 10^{-3} . However, the overall dynamics is not affected and we observe the distinct states of combustion noise, intermittency, and thermoacoustic instability.

The velocity field is evaluated using a cross-correlation algorithm with a grid-refining multipass approach and least square Gaussian fit peak search scheme³¹ available in the PIVview software (www.pivtec.com). For low flow-rates (at $\phi = 0.96$ and $\phi = 0.83$), the grid refining multipass approach is begun with 192×192 pixels with the final grid size at 32×32 pixels. A 50% overlap is used between the interrogation windows. For high flow rates ($\phi = 0.63$), the initial grid size is set at 192×192 pixels followed by 4 passes with a final grid size of 48×48 pixels to reduce the in-plane loss of correlation. At these high flow rates, 65% overlap is chosen between the interrogation windows. The grid size and the overlap are selected such that the resolution of the evaluated velocity field remains almost the same for all the flow rates. This results in a vector spacing of approximately 1 mm for all the flow rates. Ideally, at these high flow rates, the pixel displacement should be $1/4^{\text{th}}$ of the size of the interrogation windows for the PIV evaluation. Due to the medium density of the seeding particles, we cannot decrease the size of the interrogation windows as the number of seeding particles becomes less. At the same time, higher density of seeding causes faster clouding. Hence, we are restricted in choosing 48×48 as the size of the interrogation windows for the high flow rates. This could result in more outliers.

Post-processing algorithms are used to detect and replace spurious vectors. The maximum displacement test is used with appropriate thresholds for different flow rates to detect spurious vectors.³¹ These thresholds are selected based on the expected bulk flow velocities. Further, a vector difference filter³¹ calculating the magnitude of the vector difference of a vector to each of its 8 neighbours also detects spurious vectors. A threshold of 2 pixels is selected for this filter. In total, less than 1% of the total velocity vectors are detected as spurious vectors and replaced with a bilinear interpolation method. The bulk of the uncertainty from the PIV evaluation is a result of the short pixel displacement. Sub-pixel estimation accuracies of the order of $1/10^{\text{th}}$ to $1/20^{\text{th}}$ of a pixel are realistic for 32×32 pixel samples from 8-bit digital images.³¹ This results in a velocity uncertainty between 1.25% and 2.5% for low flow rates where the size of interrogation windows is 32×32 pixels. The uncertainty in the velocity measurements could rise to 5% due to the use of 48×48 pixels for high flow rates. Furthermore, particle displacement in the

recirculation and wake regions are approximately 0.2 pixels, which results in velocity uncertainties of 50% as the sub-pixel displacement is 0.1 pixels.

III. METHODS

A. Finite time Lyapunov exponent (FTLE)

Lagrangian coherent structures or LCS, by definition, are the strongest repelling, attracting, or shearing material surfaces in the flow over a finite time interval.²¹ A popular technique to extract LCS from the flow-field is by tracking the ridges (or the contours of maxima) in the field of what are known as Finite Time Lyapunov Exponents (FTLEs). FTLEs are the unsteady, finite-time extensions of stable and unstable manifolds defined for an autonomous dynamical system.^{21,33}

In the flow field of a dynamical system, fluid parcels converge along material surfaces termed unstable manifolds and diverge across material surfaces termed stable manifolds. The fluid parcel stretches across the stable manifold and eventually assumes the shape of the unstable manifold.

For an autonomous system, the Lyapunov exponents, which measure the rate of separation of neighbouring fluid parcels as they are advected by the flow-field, remain invariant with time. The ridges in the Lyapunov exponent field so computed reveal the stable manifolds. Unstable manifolds are obtained when the separation is tracked backwards in time; i.e., attracting trajectories in forward time act as repelling trajectories in backward time. Since Lyapunov exponents are not invariant for an unsteady system where the flow-fields keep changing with time (as is usually the case in combustor flow-fields), one uses finite-time Lyapunov exponents (FTLEs) to obtain manifolds of attracting and repelling trajectories. The ridges of this FTLE field are labelled Lagrangian Coherent Structures (LCS). When the particles are advected backwards in time, the ridges of FTLE field represent an approximation to coherent structures (or attracting LCS) in the flow-field.³⁴

To compute the FTLE, one tracks the displacement of a given fluid parcel x at time t as a function of a known reference initial position x_0 and initial time t_0 . Such a mapping, referred to as the flow map, is performed for each point in the flow-field as: $F_{t_0}^t(x_0) := x(t; t_0, x_0)$. Once the position of fluid parcels at time t is known, the Jacobian of the local flow map $\nabla F_{t_0}^t(x_0)$ that gives the volumetric change in deformation of fluid parcels is found. Then, one obtains the right Cauchy-Green tensor defined as

$$C_{t_0}^t(x_0, t_0) = \left[\nabla F_{t_0}^t(x_0) \right]^\dagger \nabla F_{t_0}^t(x_0). \quad (1)$$

Here, \dagger represents the transpose operation. The Cauchy-Green tensor $C_{t_0}^t(x_0, t_0)$ is a matrix that represents the square of the local change in distance due to deformation. It is a square matrix of dimension equal to the number of vector directions under consideration; i.e., for a 2D flow-field, $C_{t_0}^t(x_0, t_0)$ is a 2×2 matrix. The largest eigenvalue of

Cauchy-Green tensor $C_{t_0}^t(x_0, t_0)$ is related to the finite-time Lyapunov exponent field $\sigma_{t_0}^T(x_0, t_0)$ as

$$\sigma_{t_0}^T(x_0, t_0) = \frac{1}{|T|} \ln \sqrt{\lambda_{\max}(C_{t_0}^t(x_0, t_0))}. \quad (2)$$

Here, $\sigma_{t_0}^T(x_0, t_0)$ quantifies the rate of separation of the neighboring trajectories of fluid parcels which were initially close and $T = t - t_0$ represents the time interval of parcel advection. The ridges in the FTLE field indicate the maximal repelling material surfaces (or forward-time LCS) in the flow field over the finite time interval T . The attracting LCS is usually estimated as the maximal repelling LCS by performing the particle advection backwards in time. In the present manuscript, these attracting LCS of the backward-time FTLE fields (referred as bFTLE hereafter) are computed to obtain the coherent structures that are present in the flow field at the instants of large amplitude sound generation.

As is evident from Eq. (2), the ridges of LCS are sensitive to the choice of the time interval T . An optimum time interval T_0 is determined ensuring that sufficient number of frames required to fully resolve the coherent structures are retained without compromising the ability to capture the flow physics. If the time interval is not adequate, the structures are not well resolved. The approximation of exponential separation of trajectories [Eq. (2)] becomes inappropriate if the time interval is too large. We find that the results are robust over a range of T close to T_0 .

Once the optimum time interval T_0 is selected, a sliding window approach is employed to obtain the variation of LCS as a function of time. For instance, given T_0 , the fluid parcels are advected from the first time instant ($t = t_1$) until they reach some position after the optimum time interval ($t = t_1 + T_0$). Then, the LCS are determined for time t_0 using the procedure outlined earlier. The whole procedure is then repeated by advecting the fluid parcels from the second time instant ($t = t_2$) to $t = t_2 + T_0$ and so on.

B. Dynamic mode decomposition (DMD)

The velocity field acquired from experiments or numerical simulations often contain dynamics occurring over a range of frequencies with some amount of noise. Therefore, to extract the coherent structures at a particular frequency, an appropriate flow-decomposition technique such as Dynamic Mode Decomposition (DMD) can be used.^{29,35} Each DMD mode represents a basis function that characterizes a particular frequency in the flow-field. To obtain the DMD modes, snapshots of the velocity field ($U_x(t), U_y(t)$) are acquired over N consecutive instants of data acquisition. These snapshots are then stored in two snapshot matrices V_1^{N-1} and V_2^N as follows:

$$\mathbf{v}_j = \begin{bmatrix} U_x \\ U_y \end{bmatrix}_j, \quad (3a)$$

$$V_1^{N-1} = \{v_1, v_2, v_3, \dots, v_{N-1}\}, \quad (3b)$$

$$V_2^N = \{v_2, v_3, v_4, \dots, v_N\}, \quad (3c)$$

where v_j represents the j^{th} velocity snapshot. Then, we represent the snapshot matrices using the relation

$$V_2^N = AV_1^{N-1}. \quad (4)$$

The DMD frequencies and the corresponding modes are the eigenvalues and eigenvectors of A .³⁶ However, solving A as an eigenvalue problem to obtain the DMD modes is numerically expensive. Therefore, Eq. (4) is rearranged in a different manner to extract the modes as follows:

As a first step, singular value decomposition (SVD) of the velocity snapshot matrix V_1^{N-1} is performed as $V_1^{N-1} = U\Sigma W^\dagger$; here, U contains the dynamics modes. Both U and W are orthonormal matrices and Σ is a diagonal matrix containing the singular values of the snapshot matrix V_1^{N-1} . A companion matrix S having the same eigenvalues and eigenvectors as matrix A is formed using the similarity transformation $S = U^\dagger AU$. After substituting for A using Eq. (4), the expression for the companion matrix becomes $S = U^\dagger V_1^N W \Sigma^{-1}$. The eigenvalue matrix D and the eigenvector matrix Y of S are then calculated to obtain the DMD frequencies and the corresponding dynamic modes. The imaginary parts of the eigenvalues give the frequencies of the DMD modes and the real parts give the corresponding growth rates. Using the eigenvectors Y_j , the normalized dynamic modes ψ_j are then found as follows:

$$Z_j = W \Sigma^{-1} Y_j, \quad (5)$$

$$\hat{Z}_j = \frac{Z_j}{|Z_j|}, \quad (6)$$

$$\psi_j = V_1^{N-1} Z_j. \quad (7)$$

C. Obtaining DMD time-coefficients during intermittency

For certain operating conditions of the combustor, the velocity field consists of several frequencies which rise and fall in dominance over the course of time. In other words, the amplitude of the DMD modes corresponding to these frequencies change with time. The DMD procedure outlined previously cannot take into account such amplitude variations. Therefore, a modified approach which was proposed recently by Alenius^{25,37} was utilized to obtain the temporal variations of the DMD modes.

Velocity at a particular time instant can be expressed in terms of the DMD modes ψ_j as

$$\mathbf{v}(\mathbf{x}, t) = \sum_{j=0}^{\infty} \psi_j(\mathbf{x}) \mathbf{a}_j(t), \quad (8)$$

where $\mathbf{a}_j(t) = [a_0(t), a_1(t), \dots, a_p(t)]^\dagger$ represent the time coefficients of the DMD modes or the strength of the DMD mode at time t . In regimes where the flow-field is dominated by a finite number of modes (frequencies) of varying amplitudes, the entire flow-field can be expressed in terms of the DMD modes corresponding to these dominant modes. In other words, a finite number of DMD modes span the velocity field. Under such circumstances, the time coefficients for these dominant

DMD modes can be computed using the least squares method by solving Eq. (8) at various time instants t_i .

While calculating the coefficients, eigenvectors are considered to be orthogonal to each other which is an approximation.³⁸ However, this orthogonality often holds true as can be verified by performing a Fourier transform on the time coefficients. In the present study, we observe that the characteristic frequency of the DMD mode is retained in the time coefficients even after assuming orthogonality. The decomposed velocity-field at a particular frequency is then obtained as

$$v_i^j(\mathbf{x}, t_i) = \psi_j(\mathbf{x})a_j(t_i). \tag{9}$$

In Sec. IV, implementation of these methods to velocity data obtained from a bluff-body stabilized combustor is discussed in detail.

IV. RESULTS AND DISCUSSION

A. Identification of combustion regimes

Experiments are performed on the bluff-body stabilized combustor at different air flow rates corresponding to different mean burner velocities V_0 by keeping the mass flow rate of fuel at a constant value of 0.5 g/s. Simultaneous measurements of pressure and velocity are acquired at these air flow rates for a duration of 1.364 s at sampling rates of 10 kHz and 1 kHz, respectively. The dominant frequencies in pressure and velocity data obtained using FFT are plotted as a function of the mean velocity in the burner in Fig. 2. The velocity signal is obtained as the resultant of the mean velocity components computed over all the grid points. The mean of the velocity signal is then subtracted from the velocity signal before performing FFT.

At low mean flow velocities corresponding to the combustion noise regime, there are no visible peaks in amplitude spectra of pressure and velocity (see the left panel of Fig. 2). As the mean flow velocity is increased, two frequencies emerge, one which is dominant in the velocity signal at $f_h = 30.7$ Hz

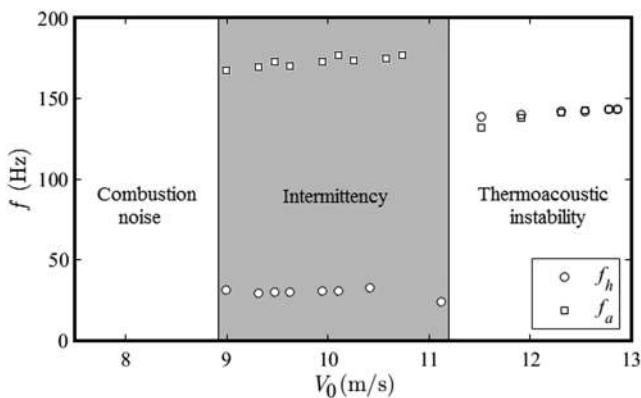


FIG. 2. The dominant frequencies in the pressure signal (f_a) and the velocity signal (f_h) as a function of the mean velocity V_0 through the burner. Peaks below 4 Pa in pressure and 0.001 m/s in velocity are not considered in the selection of dominant frequencies.

and the other which is dominant in the pressure signal at $f_a = 176.4$ Hz (see the middle panel of Fig. 2). After a critical value of the mean burner velocity, the dominant peaks in the pressure and velocity spectra become equal ($f = 141.9$ Hz) and the dynamics enters the regime of thermoacoustic instability (see the right panel of Fig. 2).

The region where two distinct dominant frequencies are observed in the dynamics is marked in grey in Fig. 2. This region has previously been described as the intermittent regime in the literature, characterized by bursts of high-amplitude periodic oscillations in pressure that emerge almost randomly from a background of aperiodic fluctuations.⁵ We also observe that both frequencies f_h and f_a are present in the spectra of pressure and velocity signals during intermittency; however, the dominant frequency in velocity is f_h , whereas f_a is dominant in the pressure signal.

To understand the role of the frequencies f_h and f_a in the establishment of large-amplitude oscillations in the combustor, DMD modes are obtained from the PIV data acquired in the three regimes corresponding to mean burner velocities of 8.7, 10.1, and 12.3 m/s, respectively (see Table I). The amplitude spectra of pressure and velocity in these regimes are shown in Fig. 3 (top and center panels). The variation of the norm of the dynamic modes with frequency is shown in the bottom panel. As expected, the norm of the DMD modes shows no peaks in the combustion noise regime. As the dynamics enters the intermittent regime, there are two distinct peaks at $f_h = 30.7$ Hz and $f_a = 176.4$ Hz, respectively. The modes associated with these frequencies, identified as the dominant frequencies in the velocity and pressure spectra, will hereafter be described as the hydrodynamic mode and the acoustic mode, respectively. It should be noted that the DMD spectra clearly shows the presence of two dominant modes unlike the spectra of pressure and velocity signals. Therefore, it is a convenient method to identify the start of the intermittent regime from the set of operating conditions explored. In the thermoacoustic instability regime, the norm of DMD modes shows a single peak at the instability frequency of $f = 141.9$ Hz which matches the peaks found in the pressure and velocity spectra.

We wish to comment that the amplitude spectra of heat release rate fluctuations (not shown) also have peaks at the same frequencies as observed in the amplitude spectra of velocity fluctuations. Since our primary objective is to identify feedback mechanisms in the flow-field, we restrict our analysis to velocity and pressure fields. Due to the direct coupling that exists between velocity and heat release rate

TABLE I. Selected parametric values corresponding to the operating conditions studied. Velocity data were sampled at 1 kHz and pressure data at 10 kHz at all operating conditions.

	ϕ	V_0 (m/s)	f (Hz)
Combustion noise	0.90	8.7	...
Intermittency	0.77	10.1	30.7, 176.4
Thermoacoustic instability	0.63	12.3	141.9

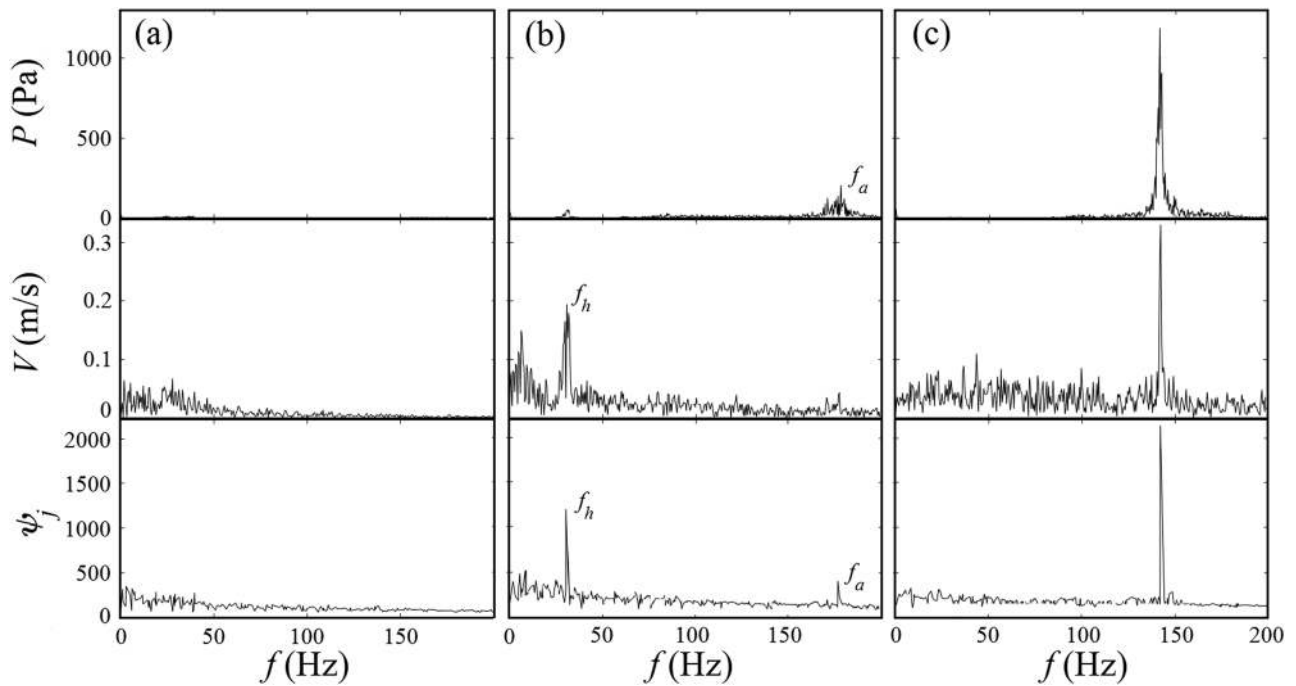


FIG. 3. The amplitude spectra of the pressure signal $P(f)$ (top) and the velocity signal $V(f)$ (middle) and the norm of the DMD modes $\Psi_j(f)$ (bottom) in the regime of (a) combustion noise ($\phi = 0.90$, $V_0 = 8.7$ m/s), (b) intermittency ($\phi = 0.77$, $V_0 = 10.1$ m/s), and (c) thermoacoustic instability regime ($\phi = 0.63$, $V_0 = 12.3$ m/s).

fluctuations in such combustors, the contribution of the heat release rate in the mechanisms leading to thermoacoustic instability is, therefore, implicitly accounted for in considering the interactions between the unsteady pressure and velocity fields.

The presence of two dominant frequencies during the intermittent regime is in line with the mechanism proposed in Nair, Thampi and Sujith⁵ and Nair and Sujith³⁹ that at least two distinct time scales are required to describe intermittency. One is a fast, acoustic time scale (represented by the peak in the pressure spectra) which depends on the travel time of sound in the combustion chamber and the other is a slower, hydrodynamic time scale (represented by the peak in the velocity spectra) representing periodic flow-features such as vortex shedding that depend on the flow velocity inside the combustion chamber. When a phase lock-in occurs between dynamics happening over these two distinct time scales, large-amplitude oscillations are established in the combustion chamber. Since intermittency occurs as a precursor regime to thermoacoustic instability, if the mechanism of sound production can be identified in the intermittent regime itself, appropriate control action (active or passive) may be taken to prevent the onset of thermoacoustic instability.

The DMD time coefficients for the hydrodynamic mode (a_1) and the acoustic mode (a_2) are shown in Figs. 4(a) and 4(b), respectively. Figure 4(c) shows the phase difference $\Delta\Phi$ between the two modes obtained using Hilbert transform

and plotted as a function of time. We see that regions of periodic bursts in the pressure signal correspond to time intervals where the total phase difference grows linearly with

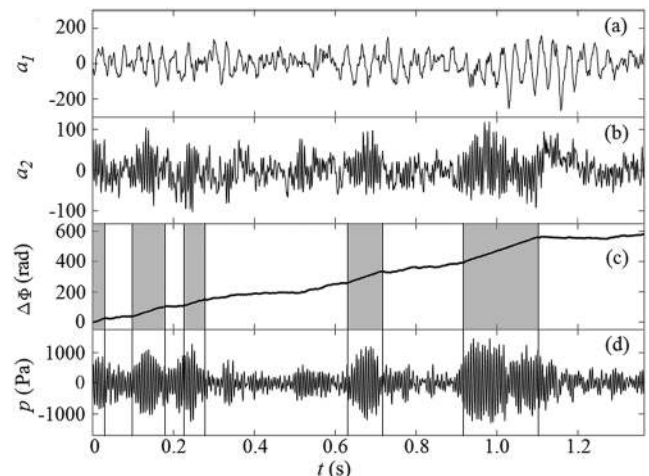


FIG. 4. DMD time coefficients of (a) the hydrodynamic mode a_1 corresponding to dynamics at $f_h = 30.7$ Hz and (b) the acoustic mode a_2 corresponding to dynamics at $f_a = 176.4$ Hz in the intermittent regime ($\phi = 0.77$, $V_0 = 10.1$ m/s). (c) Total phase difference between the acoustic and the hydrodynamic modes ($\Delta\Phi = \Phi_{a_2} - \Phi_{a_1}$) obtained using a Hilbert transform and (d) the corresponding unsteady pressure signal are also shown. The grey boxes represent time intervals where intermittent burst oscillations are observed. They also correspond to a linear increase in $\Delta\Phi$.

time [refer to Fig. 4(d) and grey boxes in Fig. 4(c)]. In other words, in these time intervals, the difference in the frequencies Δf is a constant. Further, the slope of the phase difference during these instants of periodic bursts are related to the frequencies f_h and f_a through the relation

$$\frac{d\Delta\Phi}{dt} = \frac{1}{2\pi}(f_a - f_h). \tag{10}$$

In this relationship, it should be noted that the phase of the Hilbert transform is $\Phi = 2\pi f + \phi(t)$, where f is the frequency of the signal and $\phi(t)$ the arbitrary time-varying phase. When $\Delta\Phi$ varies linearly as in Eq. (10), it implies that $\Delta\phi$ is a constant. This relationship corroborates that a phase lock-in between the hydrodynamic and the acoustic modes is responsible for the periodic high-amplitude bursts observed during intermittency. The pressure fluctuations grow in amplitude when the acoustic and the hydrodynamic modes have a favourable phase relationship. This phase-locking then persists for a short duration. Eventually, the two modes move out of phase and the amplitude of the pressure fluctuations decay.

We suspect that this moving in and out of phase happens as the frequencies of the hydrodynamic (f_h) and acoustic modes (f_a) are close to commensurate. When the phase of the two modes comes arbitrarily close, a lock-in happens which is sustained until the dynamics drifts the phase apart. An intermittent phase synchronization was also reported between the pressure and heat release rate fluctuations for the same combustor in the intermittent regime.⁴⁰ Since there is a direct coupling between velocity and heat release fluctuations for such combustors, this should come as no surprise.

The DMD modes corresponding to the acoustic mode at 176.4 Hz (f_a) and the hydrodynamic mode at 30.7 Hz (f_h) are shown in Figs. 5(a) and 5(b). We see that the acoustic mode is dominant in the region upstream of the bluff-body whereas the hydrodynamic mode is dominant downstream of the bluff-body. In other words, dynamic processes ultimately responsible for sound production happen primarily upstream in the region between the dump plane and leading edge of the bluff-body.

B. Computing bFTLE fields

To identify the coherent structures responsible for sound production, the FTLE methodology outlined in Sec. III is

applied to the PIV data acquired in the regime of thermoacoustic instability ($\phi = 0.63$, $V_0 = 12.3$ m/s) and intermittency ($\phi = 0.77$, $V_0 = 10.1$ m/s).

1. LCS of thermoacoustic instability

In Fig. 6, the bFTLE fields computed over a cycle of thermoacoustic instability are shown along with the corresponding pressure signal. The dynamics observed during instability consists of three dominant features: (1) shear layer roll-up in the dump plane followed by its convection and impingement on the combustor walls, (2) a separated shear layer originating at the leading edge of the bluff body and convecting downstream, and (3) vortex roll-up and shedding in the bluff-body wake augmented by the separating shear layer. As the unsteady pressure increases and reaches the local maxima (compression phase), the shear layer separating from the dump plane rolls up and moves towards the bluff-body [refer to Figs. 6(a)–6(d)]. The increase in pressure also commences the roll-up of a vortex from the leading edge of the bluff-body. The two shear layers squeeze the fluid in between them at the point of pressure maxima. As the pressure starts decreasing from the maxima towards the minima (expansion phase), the vortex formed upstream of the bluff-body impinges on the combustor walls [refer to Figs. 6(e)–6(g)]. During this time instant, the vortex formed at the leading of the bluff-body grows to its maximum size and sheds downstream. Due to the impingement of flame carrying vortex from the dump plane, there is an increase in heat release rate and consequently a rise in pressure due to fine-scale mixing and burning which initiates the start of a new cycle.

2. LCS of intermittent regime

To identify the flow structures observed exclusively during sound production, we first consider a time interval within the periodic bursting stage of intermittency. In Fig. 7, the evolution of the bFTLE field over a cycle of burst oscillation in pressure is shown. Time coefficients for the two modes are shown in the left and the corresponding pressure signal on the right of the panels. Over this short time duration, the variations in the hydrodynamic mode coefficient a_1 are negligible whereas the variation in acoustic mode coefficient a_2 is periodic. Although the shear layer dynamics happen at the same frequency as that of pressure fluctuations, there need not be a good correlation between the two processes. This is because the phase difference between the acoustic part of the

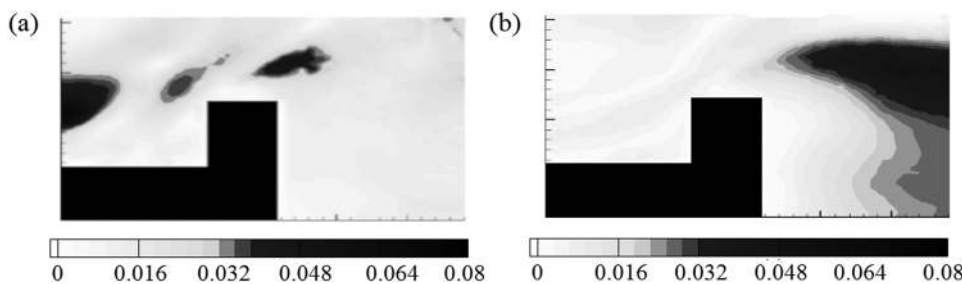


FIG. 5. The DMD mode at (a) $f_a = 176.4$ Hz (acoustic mode), and (b) $f_h = 30.7$ Hz (hydrodynamic mode) in the intermittent regime ($\phi = 0.77$, $V_0 = 10.1$ m/s). Flow is from left to right.

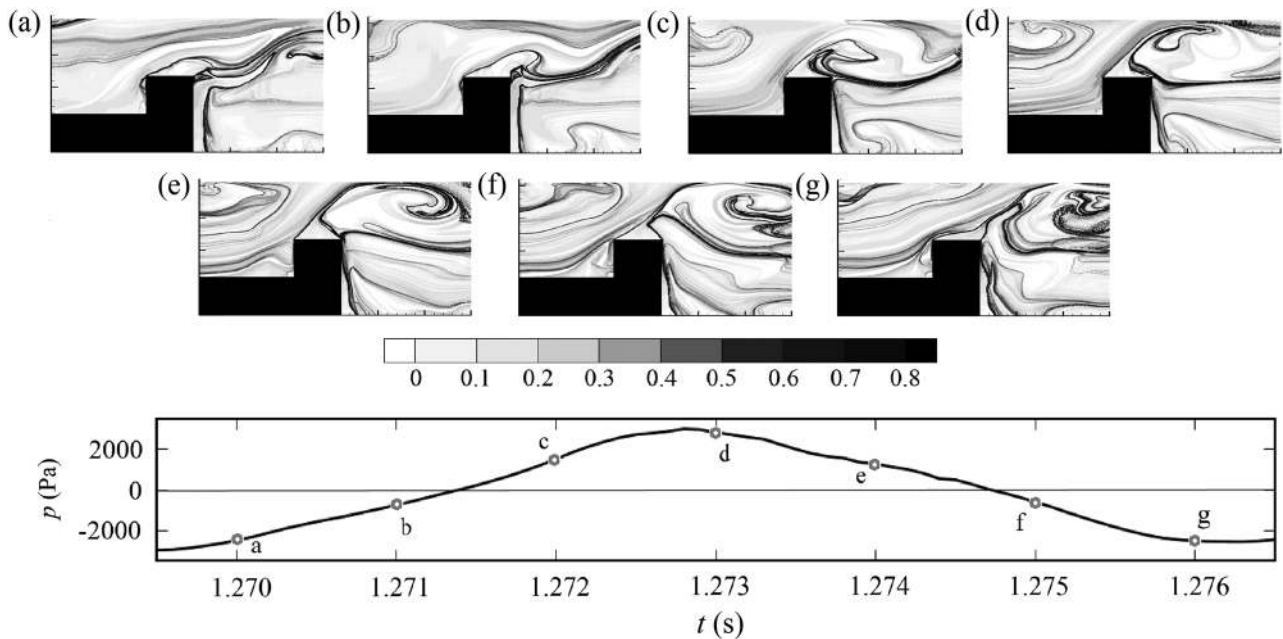


FIG. 6. bFTLE fields (panels) computed from the velocity fields along with the corresponding pressure data (bottom) over a time period of thermoacoustic instability ($\phi = 0.63$, $V_0 = 12.3$ m/s, $T_0 = 16$ ms). The bFTLE fields show periodic shear layer roll-up and impingement upstream of the bluff-body, shear layer separation from the leading edge of the bluff-body, and vortex shedding downstream of the bluff-body. Flow is from left to right.

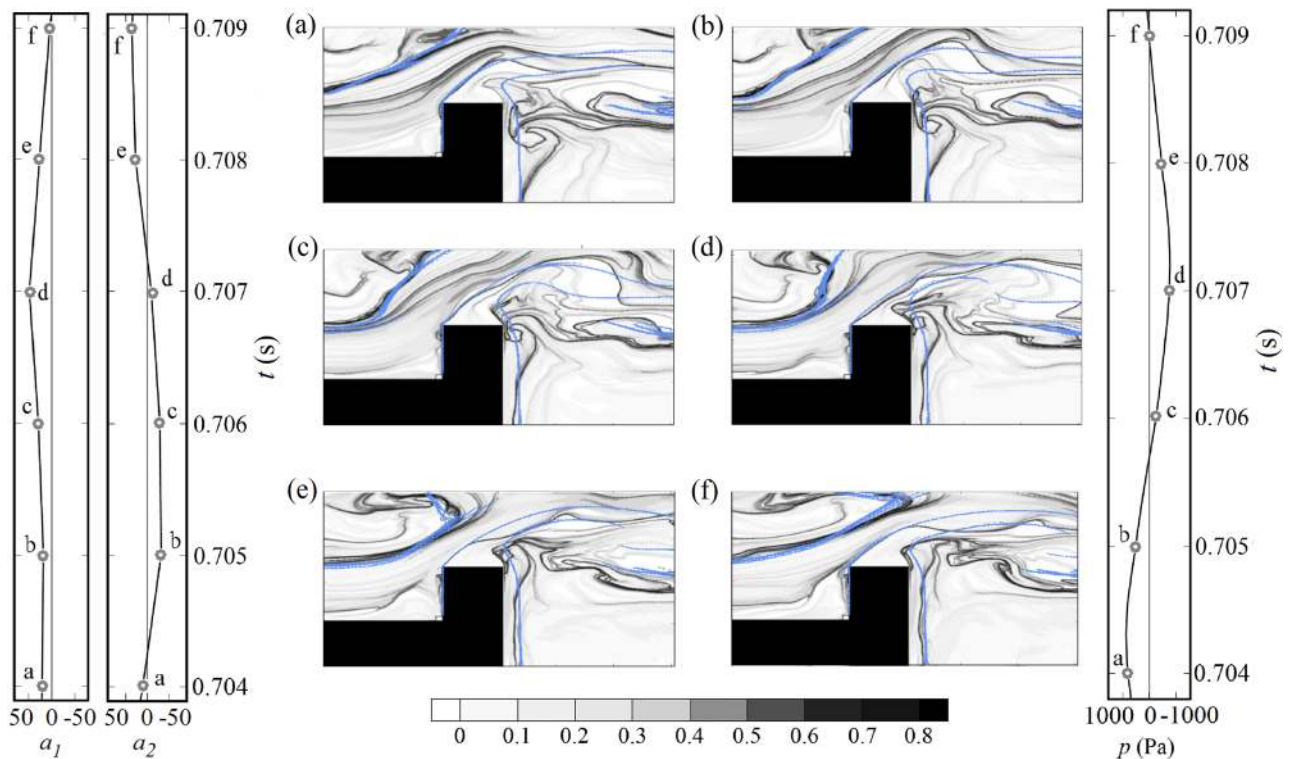


FIG. 7. bFTLE fields (contour) computed during an intermittent bursting cycle ($\phi = 0.77$, $V_0 = 10.1$ m/s, $T_0 = 16$ ms) along with the instantaneous pressure signal (right) and time coefficients a_1 and a_2 (left). Ridges of the bFTLE fields computed using a DMD-filtered velocity data comprising the mean flow and the acoustic field are overlaid in blue. A good match is obtained between the ridges of both the bFTLE fields showing shear layer flapping back and forth and impinging on the combustor walls. Flow is from left to right.

flow field and the pressure fluctuations can assume arbitrary values due to the drifting of phase in the windows without bursts.

Over a burst cycle, the shear layer upstream of the bluff-body, which separates the cold reactants and the hot products moves away from the bluff-body towards the dump plane when a_2 moves towards a local minimum [refer to Figs. 7(a)–7(c)] and towards the bluff-body from the dump plane when a_2 moves towards a local maximum [refer to Figs. 7(d)–7(f)]. Correspondingly, the shear layer separating from the leading edge of the bluff-body tilts slightly downstream when the pressure decreases and slightly upstream when the pressure increases due to the propagation of periodic convective waves along the shear layer. The net result is a periodic squeezing of the two shear layers together just as we observed for thermoacoustic instability.

In order to establish that the observed structures are truly acoustic in nature, we created an artificial flow-field by superposing the DMD modes corresponding to the mean component and the component corresponding to the acoustic mode. The ridges of the bFTLE fields obtained using this flow-field are marked in blue in Fig. 7. We observe that the prominent flow features identified using the overall velocity field; i.e., the roll up of the shear layer from the dump plane and leading edge of the bluff-body are still present in this artificial flow field. This indicates that the identified dynamics of flow structures observed during sound production are indeed acoustic.

We wish to state that computing bFTLE fields directly from the individual filtered velocity components (for instance, the acoustic mode) would be usually incorrect. This is because DMD is an Eulerian flow decomposition technique whereas FTLE computation is Lagrangian, two methods that do not

commute. The good similarity observed in the sets of bFTLE fields computed using unfiltered and DMD filtered data sets therefore is indicative of the negligible effect the hydrodynamic mode plays in the overall dynamics of bursting over a cycle (as it happens over a larger time scale). We further note that the vortex shedding which was downstream of the bluff-body during instability is not a prominent feature of the dynamics during bursting. We suspect this vortex shedding to be the flow structure corresponding to the hydrodynamic mode. This is supported by the DMD mode shape obtained for the hydrodynamics frequency f_h which shows significant activity downstream of the bluff-body with negligible contributions upstream [refer to Fig. 5(b)]. The flapping of the shear layer when phased properly with the vortex shedding process downstream of the bluff-body results in the growth of oscillations during the bursting cycle.

To further substantiate our proposition, we compute the bFTLE fields over a same interval when the pressure amplitudes are low without bursts (refer to Fig. 8). We clearly see that unlike the previous case, there is no periodic shear layer flapping from the dump plane or the leading edge of the bluff-body. The changes in the ridges across the time interval are marginal and there is no periodic process which can lock in with the hydrodynamic mode. This highlights the usefulness of the DMD filtering in identifying the sound producing dynamics of the flow structures.

Based on these observations, we can conclude that the acoustic mode is responsible for the shear layer roll-up, convection and subsequent impingement upstream of the bluff body. The hydrodynamic mode plays a negligible role in this process in the time scale considered. When one of the acoustic modes is excited, a periodic fluctuation in heat release

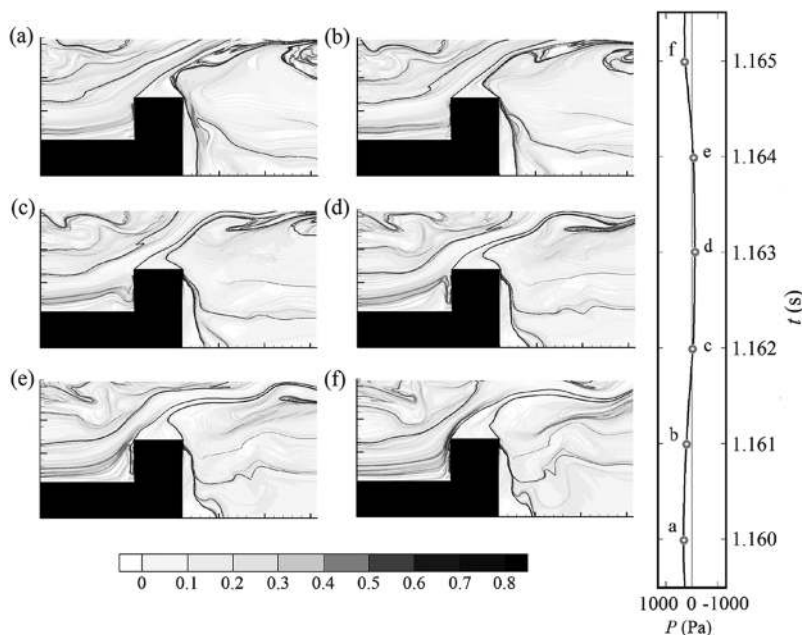


FIG. 8. bFTLE fields (panels) computed in a time window where there are no bursts in the intermittency regime ($\phi = 0.77$, $V_0 = 10.1$ m/s, $T_0 = 16$ ms) along with the instantaneous pressure signal (right). bFTLE fields show little variation across the time interval upstream of the bluff-body. Flow is from left to right.

is established at the same frequency through impingement of flame carrying vortices on the combustor walls. Periodic fluctuations in heat release rate, in turn, produce periodic pressure fluctuations that initiate a new cycle of shear layer flapping and impingement from the upstream dump plane. The strength and the existence of such a feedback necessitates a phase coupling between the acoustic and hydrodynamic modes. When the operating conditions are such that the interaction between the hydrodynamic mode and one of the acoustic modes are in phase, we have intermittent burst oscillations. When the operating conditions are such that the favourable phase relationship can be maintained over long time intervals, thermoacoustic instability is established.

It is worth noting that the aspect ratio of the bluff body; i.e., the ratio of the streamwise thickness to its diameter, has a strong effect on the shear layer.^{41,42} In the present experiment, the upstream sting that holds the bluff body adds to the thickness of the boundary layer that eventually separates at the sharp corner of the bluff body. This is important because the vortex patterns observed and the regions of intense heat release which are anticipated to reside within the vortex cores and in the Taylor layers in the braids between the vortices established by the separated shear layers can depend critically on the dimension of the bluff-body employed.⁴³ Consequently, the flow conditions at which instability is observed can also depart from the conditions reported in the study for alternate configurations of the flame holder.

Studying the flow-fields obtained during thermoacoustic instability provides limited information as separation of the role of hydrodynamic and acoustic modes is difficult. By splitting the dynamics occurring in the intermittent regime into intervals with and without sound production, we could better understand the dynamic flow features observed exclusively during sound production for the combustor under study. A suitable extension of the study would be to perform control studies where such flow structures are actively targeted and disrupted in an attempt to mitigate instability.

V. CONCLUSIONS

Coherent structures are often the cause of thermoacoustic instability in gas turbine combustors. Hence, identifying the mechanisms and the positive feedback processes connecting the flow-field, heat release rate, and the acoustics during early stages of design is critical in effecting appropriate control action to prevent the onset of thermoacoustic instability. This paper outlines a novel methodology incorporating a flow decomposition technique (DMD) and a vortex detection scheme (bFTLE) to identify the thermoacoustic instability mechanism from flow-field measurements. The DMD algorithm allows resolving the flow-field into components corresponding to the dominant frequencies at various operating conditions. Studying the bFTLE fields on such DMD-resolved velocity data in carefully chosen time intervals then allows the flow structures observed exclusively during sound production to be identified.

This framework is applied to experimental velocity fields obtained from a bluff-stabilized combustor in the dynamic regimes of combustion noise ($\phi = 0.90$, $V_0 = 8.7$ m/s), intermittency ($\phi = 0.77$, $V_0 = 10.1$ m/s), and thermoacoustic instability ($\phi = 0.63$, $V_0 = 12.3$ m/s). A clear picture of the bifurcation of the dynamics into these three regimes is presented as a function of the mean velocity through the burner. It is shown that the intermittent regime emerges as the result of mutually-coupled dynamics operating over two distinct, dominant time scales: a faster, acoustic time scale and a slower, hydrodynamic time scale. Utilizing the norm of the DMD modes, it is possible to identify the starting point of the intermittent regime.

bFTLE fields during thermoacoustic instability show that the dominant dynamics are the shear layer roll-up, convection and impingement upstream of the bluff-body, and vortex shedding downstream of the bluff-body. Two dominant frequencies were observed in the intermittent regime: 30.7 Hz corresponding to the hydrodynamic mode and 176.4 Hz corresponding to acoustic mode. These two modes lock in- and out of phase resulting in the formation and disruption of periodic bursts during intermittency. We find that the bFTLE fields during the bursting stage of intermittency retain qualitative similarity with those obtained during instability. Further, using a DMD filtered velocity comprising only of the mean and the acoustic velocities, we find that the critical dynamic features that were identified—the shear layer flapping in the dump plane and from the leading edge of the bluff-body—are retained. We also confirm that these dynamics are absent in a time interval when the pressure amplitudes are low. This convincingly demonstrates that it is possible to identify flow structures corresponding to the acoustic mode from velocity data comprising multiple modes at an early stage. Further, the study strongly indicates that a lower order representation of the dynamics is possible to describe the state of intermittency, which will be taken up in a future study.

It is already known that thermoacoustic instability is established when there is a favourable phase relationship between the hydrodynamic and acoustic modes; i.e., when the frequencies of the hydrodynamic mode and the acoustic mode become commensurate. The analysis carried forth in the study shows that these modes can be identified well in advance of an impending instability. bFTLE fields reveal the flow structures one can expect to observe during thermoacoustic instability without actually conducting costly experiments in such regimes. The presented framework can, therefore, be implemented during the early design stages of various combustion chambers to mitigate large-amplitude pressure oscillations.

ACKNOWLEDGMENTS

C. P. Premchand and Vineeth Nair would like to thank IRCC, IIT Bombay, for funding the study (Grant No. 16IRCCSG006). N. B. George, M. Raghunathan, V. R. Unni, and R. I. Sujith are thankful to Office of Naval Research Global (ONRG) for their financial support.

REFERENCES

- ¹T. Lieuwen and V. Yang, *Combustion Instabilities in Gas Turbine Engines: Operational Experience, Fundamental Mechanisms, and Modeling* (American Institute of Aeronautics and Astronautics, 2005).
- ²F. E. C. Culick, "Unsteady motions in combustion chambers for propulsion systems," AGARDograph RTO-AG-AVT-039, 2006.
- ³J. W. S. Rayleigh, "The explanation of certain acoustical phenomena," *Nature* **18**, 319–321 (1878).
- ⁴T. Lieuwen, "Combustion driven oscillations in gas turbines," *Turbomach. Int.* **44**(1), 16–18 (2003).
- ⁵V. Nair, G. Thampi, and R. I. Sujith, "Intermittency route to thermoacoustic instability in turbulent combustors," *J. Fluid Mech.* **756**, 470–487 (2014).
- ⁶V. Nair and R. I. Sujith, "Multifractality in combustion noise: Predicting an impending combustion instability," *J. Fluid Mech.* **747**, 635–655 (2014).
- ⁷J. Tony, E. A. Gopalakrishnan, E. Sreelekha, and R. I. Sujith, "Detecting deterministic nature of pressure measurements from a turbulent combustor," *Phys. Rev. E* **92**, 062902-1–062902-11 (2015).
- ⁸V. Nair, G. Thampi, S. Karuppusamy, S. Gopalan, and R. I. Sujith, "Loss of chaos in combustion noise as a precursor of impending combustion instability," *Int. J. Spray Combust. Dyn.* **5**, 273–290 (2013).
- ⁹H. Gotoda, H. Nikimoto, T. Miyano, and S. Tachibana, "Dynamic properties of combustion instability in a lean premixed gas-turbine combustor," *Chaos* **21**, 013124–013124-11 (2011).
- ¹⁰V. Nair and R. I. Sujith, "Intermittency as a transition state in combustion dynamics: An explanation for flame dynamics near lean blowout," *Combust. Sci. Technol.* **187**, 1821–1835 (2015).
- ¹¹V. R. Unni and R. I. Sujith, "Multifractal characteristics of combustor dynamics close to lean blowout," *J. Fluid Mech.* **784**, 30–50 (2015).
- ¹²M. P. Juniper and R. I. Sujith, "Sensitivity and nonlinearity of thermoacoustic oscillations," *Annu. Rev. Fluid Mech.* **50**, 661–689 (2018).
- ¹³G. L. Brown and A. Roshko, "On density effects and large structure in turbulent mixing layers," *J. Fluid Mech.* **64**, 775–816 (1974).
- ¹⁴W. E. Kaskan and A. E. Noreen, "High-frequency oscillations of a flame held by a bluff body," *ASME Trans.* **77**(6), 855–891 (1955).
- ¹⁵D. E. Rogers and F. E. Marble, "A mechanism for high-frequency oscillation in ramjet combustors and afterburners," *J. Jet Propul.* **26**, 456–462 (1956).
- ¹⁶J. D. Sterling and E. E. Zukoski, "Longitudinal mode combustion instabilities in a dump combustor," in AIAA 25th Aerospace Sciences Meeting, Reno, NV, 1987, Paper No. 0220.
- ¹⁷T. Poinso, A. Trouve, D. Veynante, S. M. Candel, and E. Esposito, "Vortex driven acoustically coupled combustion instability," *J. Fluid Mech.* **177**, 265–292 (1987).
- ¹⁸A. Trouve, K. Yu, and J. W. Daily, "Phase sensitive schlieren system for studying periodic combustion phenomena," in Joint Meeting of the Western States Section of the Combustion Institute, Honolulu, HI, 1987.
- ¹⁹K. C. Schadow, E. Gutmark, T. P. Parr, D. M. Parr, K. J. Wilson, and J. E. Crump, "Large-scale coherent structures as drivers of combustion instability," *Combust. Sci. Technol.* **64**, 167–186 (1989).
- ²⁰T. Peacock and G. Haller, "Lagrangian coherent structures the hidden skeleton of fluid flows," *Phys. Today* **66**(2), 41–47 (2013).
- ²¹G. Haller, "Lagrangian coherent structures," *Annu. Rev. Fluid Mech.* **47**, 137–162 (2015).
- ²²F. Beron-Vera, M. Olascoaga, and G. Goni, "Oceanic mesoscale eddies as revealed by Lagrangian coherent structures," *Geophys. Res. Lett.* **35**, L12603, <https://doi.org/10.1029/2008gl033957> (2008).
- ²³J. Peng and J. Dabiri, "Transport of inertial particles by Lagrangian coherent structures: Application to predator-prey interaction in jellyfish feeding," *J. Fluid Mech.* **623**, 75–84 (2009).
- ²⁴M. Green, C. Rowley, and A. Smits, "The unsteady three-dimensional wake produced by a trapezoidal pitching panel," *J. Fluid Mech.* **685**, 117–145 (2011).
- ²⁵V. Nair, E. Alenius, S. Boij, and G. Efraimsson, "Inspecting sound sources in an orifice-jet flow using Lagrangian coherent structures," *Comput. Fluids* **140**, 397–405 (2016).
- ²⁶I. Christov, J. Ottino, and R. Lueptow, "From streamline jumping to strange eigenmodes: Bridging the Lagrangian and Eulerian pictures of the kinematics of mixing in granular flows," *Phys. Fluids* **23**, 103302 (2011).
- ²⁷S. Benjamin, P. Ronald, F. Raphael, and T. Holger, "Ridge concepts for the visualization of Lagrangian coherent structures," *Topological Methods in Data Analysis and Visualization II*, Mathematics and Visualization (Springer, Berlin, Heidelberg, 2011), pp. 221–235.
- ²⁸R. Sampath, M. Mathur, and S. R. Chakravarthy, "Lagrangian coherent structures during combustion instability in a premixed-flame backward-step combustor," *Phys. Rev. E* **94**, 062209-1–062209-10 (2016).
- ²⁹P. J. Schmid, "Dynamic mode decomposition of numerical and experimental data," *J. Fluid Mech.* **656**, 5–28 (2010).
- ³⁰T. Komarek and W. Polifke, "Impact of swirl fluctuations on the flame response of a perfectly premixed swirl burner," *J. Eng. Gas Turb. Power* **132**, 061503-1–061503-7 (2010).
- ³¹M. Raffel, C. E. Willert, S. Wereley, and J. Kompenhans, *Particle Image Velocimetry: A Practical Guide* (Springer, 2007).
- ³²W. A. Sirignano, *Fluid Dynamics and Transport of Droplets and Sprays* (Cambridge University Press, 2010).
- ³³S. H. Strogatz, *Nonlinear Dynamics and Chaos: With Applications to Physics, Biology, Chemistry, and Engineering* (Addison-Wesley Publishing Company, 1994).
- ³⁴S. C. Shadden, F. Lekien, and J. E. Marsden, "Definition and properties of Lagrangian coherent structures from finite-time Lyapunov exponents in two-dimensional aperiodic flows," *Physica D* **212**, 271–304 (2005).
- ³⁵P. J. Schmid, L. Li, M. P. Juniper, and O. Pust, "Applications of the dynamic mode decomposition," *Theor. Comput. Fluid Dyn.* **25**, 249–259 (2011).
- ³⁶C. W. Rowley, I. Mezic, S. Bagheri, P. Schlatter, and D. S. Henningson, "Spectral analysis of nonlinear flows," *J. Fluid Mech.* **641**, 115–127 (2009).
- ³⁷E. Alenius, "Mode switching in a thick orifice jet, an LES and dynamic mode decomposition approach," *Comput. Fluids* **90**, 101–112 (2014).
- ³⁸E. Alenius, "Flow duct acoustics—An LES approach," Ph.D. thesis, Royal Institute of Technology, 2012.
- ³⁹V. Nair and R. I. Sujith, "A reduced-order model for the onset of combustion instability: Physical mechanisms for intermittency and precursors," *Proc. Combust. Inst.* **35**, 3193–3200 (2015).
- ⁴⁰S. A. Pawar, A. Seshadri, V. R. Unni, and R. I. Sujith, "Thermoacoustic instability as mutual synchronization between the acoustic field of the confinement and turbulent reactive flow," *J. Fluid Mech.* **827**, 664–693 (2017).
- ⁴¹H. Nakaguchi, K. Hashimoto, and S. Muto, "An experimental study on aerodynamic drag of rectangular cylinders," *J. Jpn. Soc. Aeronaut. Space Sci.* **16**, 1–5 (1968).
- ⁴²P. W. Bearman and D. M. Trueman, "An investigation of the flow around rectangular cylinders," *Aeronaut. Q.* **23**, 229–237 (1972).
- ⁴³J. Broadwell and R. Breidenthal, "A simple model of mixing and chemical reaction in a turbulent shear layer," *J. Fluid Mech.* **125**, 397–410 (1982).